Available online at www.sciencedirect.com

ScienceDirect

Procedia Engineering 81 (2014) 2211 – 2216

Procedia Engineering

www.elsevier.com/locate/procedia

11th International Conference on Technology of Plasticity, ICTP 2014, 19-24 October 2014, Nagoya Congress Center, Nagoya, Japan

Bursting prediction of hydroforming aluminium alloy tube based on Gurson-Tvergaard-Needleman damage model

Buang Teng*, Weinian Wang, Yinquan Liu, Shijian Yuan

National Key Laboratory for Precision Hot Processing of Metals, Harbin Institute of Technology, Harbin 150001, China

Abstract

The Gurson-Tvergaard-Needleman model was employed to predict the bursting behaviour in the hydroforming of aluminium alloy tubes. The original void volume fraction, the critical void volume fraction, and the failure void volume fraction of this model were identified by observing the damage evolution of the tensile test of 5A02 aluminium alloy with scanning electron microscopy (SEM). The other parameters of Gurson-Tvergaard-Needleman model were determined by an inverse approach which combined the uniaxial tensile test and numerical simulation. The bursting behaviour in the hydroforming of 5A02 aluminium alloy tube with different bulging length was studied by free-bulging tests and simulation based on this model. The simulation results give a good agreement with the experimentally determined bursting pressures.

Selection and peer-review under responsibility of the Department of Materials Science and Engineering, Nagoya University

Keywords: Tube hydroforming; Bursting prediction; GTN model; inverse approach

1. Introduction

Hydroforming of tube is an attractive near-net shape manufacturing technique as it can produce low weight, high strength and uniform parts while eliminating traditional stamping and welding operation. The development of hydroforming technology has led to a wide range of application in industry, especially for manufacturing high-quality lightweight components for the automobile, aviation, and aerospace industry (Yuan et al., 2011).

* Corresponding author. Tel/ fax: +86-451-86415754.
E-mail address: bgteng@hit.edu.cn

Selection and peer-review under responsibility of the Department of Materials Science and Engineering, Nagoya University
doi:10.1016/j.proeng.2014.10.310

Compared to quality steel tubes, aluminium alloy tubes are less formable. The necking criterion based on plastic instability may not predict the forming limit in a wide range of hydroforming processes. Especially, in case of aluminium alloys, the bursting failure is often observed without appearance of clear localized necking or thinning due to the low ductility (Kim et al., 2003). In general, a frequently used technique for evaluating busting failure in sheet metal forming is the forming limit diagram. However, the forming limit diagram suffers from some well-known weaknesses. It is definitely dependent on the forming history and strain path，so it can not be used to predict the formability limit in tube hydroforming, which subjects to a complicated stress state (Stoughton et al., 2004). Micromechanics have been extensively used in order to analyze and predict ductile fracture by modelling void nucleation, growth and coalescence. Gurson–Tvergaard–Needleman approach is one of well-known microscale models for ductile fracture which is extensively used for different materials and processes (Tvergaard et al., 1984). In this paper, the Gurson–Tvergaard–Needleman model was employed to analyze bursting behaviour in aluminium alloy tube hydroforming.

Nomenclature

ε_N	mean strain for nucleation
ε^P	von Mises plastic strain
f_0	original void volume fraction
f_c	critical void volume fraction
f_F	final void volume fraction
f_N	nucleating void volume fraction
K	strength coefficient
n	work hardening exponent
q_i	calibration parameter
s_N	standard deviation
σ_b	ultimate strength
σ_{eq}	von Mises equivalent stress
σ_H	hydrostatic stress
σ_y	yield stress of the matrix
δ	elongation rate

2. Damage model

In order to model the plastic flow and failure of these ductile materials, Gurson conducted an upper bound analysis of simplified models containing voids and proposed an approximate yield criterion for porous materials where the matrices obey the von Mises yield criterion, and is expressed as

$$\phi = (\frac{\sigma_{eq}}{\sigma_y})^2 + 2f\cosh(\frac{3\sigma_H}{2\sigma_y}) - (1+f^2) = 0\text{，} \tag{1}$$

where σ_{eq} is the von Mises equivalent stress, σ_y is the yield stress of the matrix, σ_H is the hydrostatic stress, and f is the volume fraction of the voids in the material.

Tvergaard introduced three calibration parameters (q_1、q_2 and q_3) into the model to adjust it to unit cell computations. The effective void volume fraction f^* was proposed by Tvergaard and Needleman to account for the onset of void coalescence:

$$\phi = (\frac{\sigma_{eq}}{\sigma_y})^2 + 2f^*q_1\cosh(\frac{3q_2\sigma_H}{2\sigma_y}) - (1+q_3(f^*)^2) = 0\text{，} \tag{2}$$

$$f^* = \begin{cases} f & \text{if } f \le f_c \\ f_c + \dfrac{1/q_1 - f}{f_F - f_c}(f - f_c) & \text{if } f_c < f < f_F \end{cases}, \tag{3}$$

where f_c is the critical value of void volume fraction at the onset of void coalescence and the final void volume fraction f_F is its value at final failure.

The evolution of the void volume fraction is expressed as the sum of void growth and nucleation:

$$\dot{f} = \dot{f}_{growth} + \dot{f}_{nucleation}. \tag{4}$$

The growth rate of voids is proportional to the hydrostatic component of the plastic strain rate, $\dot{\varepsilon}_{kk}^{p}$, as follows:

$$\dot{f}_{growth} = (1-f)\dot{\varepsilon}_{kk}^{p}. \tag{5}$$

The contribution resulting from the nucleation of new voids is assumed to be plastic strain-controlled:

$$\dot{f}_{nucleation} = \frac{f_N}{s_N\sqrt{2\pi}} \exp\left[-\frac{1}{2}\left(\frac{\varepsilon^p - \varepsilon_N}{s_N}\right)\right]\dot{\varepsilon}^p, \tag{6}$$

where f_N is the volume fraction of void nucleating particles, ε_N is the mean strain for nucleation, s_N is the standard deviation of ε_N, assuming a normal distribution in the damage model, ε^P is the von Mises plastic strain, and, $\dot{\varepsilon}^p$ is the von Mises plastic strain rate.

3. Determination of the Gurson–Tvergaard–Needleman damage model parameters

3.1. Material properties

The tube material was 5A02 (China) with 30mm diameter and 1.5mm thickness. To determine the mechanical properties of the tube, tensile specimens were cut from the tube. The chemical composition and material properties of the 5A02 aluminium alloy are presented in Tables 1 and 2, respectively. Material properties are as follows: yield stress σ_s is 88.1 MPa, tensile strength σ_b is 204 MPa, the work hardening exponent n is 0.32, elongation rate δ is 22.98%. The work hardening law is expressed $\sigma = K\varepsilon^n$, where K is the strength coefficient.

Table 1. Chemical composition of 5A02 (China).

Element	Mg	Si	Fe	Cu	Al
Wt.%	2.22	0.12	0.16	0.0012	balance

Table 2. Mechanical properties of tube used from tensile tests.

σ_s (MPa)	σ_b (MPa)	n	K(MPa)	δ (%)
83.1	204.2	0.32	441.24	22.98

3.2. Parameter identification

According to the plastic constitutive equation mentioned in the last section, nine parameters require to be identified in Gurson–Tvergaard–Needleman model: q_1, q_2, q_3, f_0, f_c, f_N, f_F, ε_N, s_N. The model coefficients proposed by Tvergaard and Needleman to amplify the hydrostatic stress effect for all strain levels are q_1 and q_2, with a reasonable constant value for metals of q_1= 1~1.5, q_2 = 1.0 and $q_3 = q_1^2$. In the present work, we assume q_1=1.5, q_2=1 and q_3=2.25. The values of void volume fraction f_0, f_c, f_F are determined by the tensile tests, which are

described by the void surface proportions obtained by the scanning electron microscope (SEM) microstructures. The values of f_N, ε_N, and s_N are determined by the inverse approach, in which the results of the load-displacement curve and the stress-strain curve are compared numerically and experimentally.

The mechanism of ductile fracture is described as a damage accumulation process. The load-displacement curve obtained from tensile test is shown in Fig.1. The corresponding locations for determining the void fraction are also presented. Image-Pro plus software is used to analyze the SEM microstructures at different deformation stages. Fig. 2 shows the microstructure of as-received 5A02 before tensile test. The original void mainly comes from the secondary phase particles. 5A02 microstructure contains Al (Mg) α grains with Mg_2Al_3 β grains decorated along the prior α grain boundaries dispersively distributed in the α matrix (Yan et al., 2014). The original void volume fraction f_0 is counted as 0.00104.

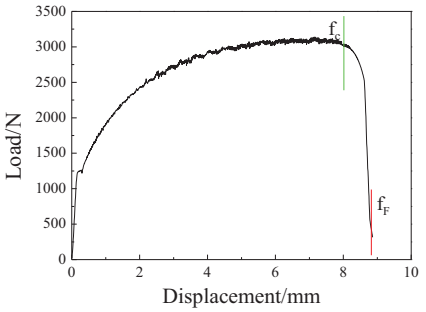

Fig. 1. Measured load-displacement curve.

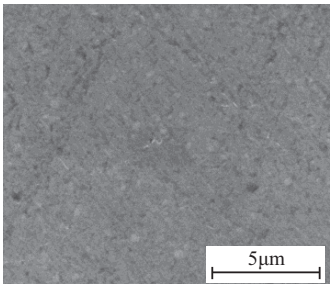

Fig. 2. Microstructure of 5A02 before plastic deformation.

Ductile fracture occurs sequentially through void nucleation, growth, and coalescence. With increasing load, the interface between α grains matrix and β particles serves as the preferable position for micro-crack nucleation and further ductile fracture. Fig. 3 presents the SEM image showing the coalescence of voids. When load increases to about 3kN, the displacement reaches 8 mm, the material carrying capacity loses quickly as some connected void bands form. Similarly, f_c is identified by area ratio and equal to 0.0196.

In the final stage of the fracture, the coalescence of voids for an increasing plastic deformation progressively reduces the material capability to support the mechanical loads up to complete failure. When displacement reaches 8.8mm, fracture occurs. The void volume fraction f_F is evaluated as 0.0363. Fig.4 presents the fracture surface, it can be seen that mainly secondary voids were found in the fracture surface.

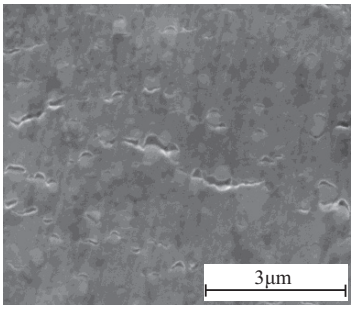

Fig. 3. SEM image showing the coalescence of voids.

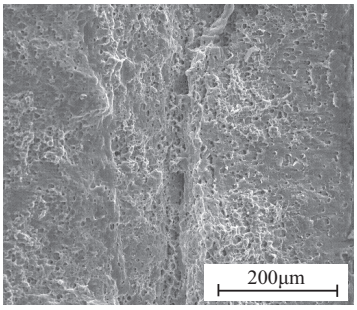

Fig. 4. SEM image showing dimples with second phase particles.

In order to determine the values of f_N, ε_N, and s_N, in Gurson–Tvergaard–Needleman model, numerical simulations of uniaxial tensile test were firstly conducted. The finite element analysis code ABAQUS 6.8 is employed. In the FE model, the specimen is modeled with solid elements (C3D8R, eight-node brick element with

reduced integration). Fig.5 and Fig.6 are comparisons of the load-displacement curve and the stress-strain curve, which obtained from experiment and simulation results with best-fit parameters. The best-fit parameters for Gurson–Tvergaard–Needleman model of 5A02 are specified in Table 3.

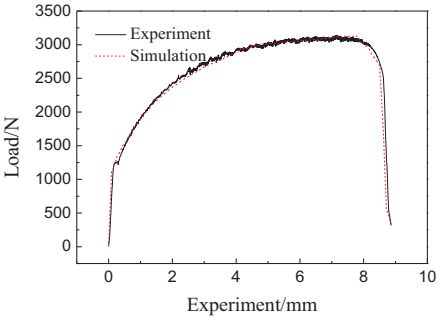

Fig. 5. Comparison of the load-displacement curve.

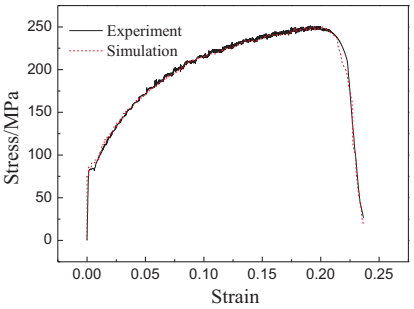

Fig. 6. Comparison of the stress-strain curve.

Table 3. Determined parameters of Gurson–Tvergaard–Needleman model.

q_1	q_2	q_3	f_0	f_c	f_F	ε_N	s_N	f_N
1.5	1	2.25	0.001	0.02	0.0363	0.1	0.1	0.0242

4. Bursting prediction of free-bulging aluminium alloy tube

Fig.7 shows the main parts of the experimental setup. Both of upper and lower dies consist of two parts, so the bulging length can be adjusted, the bulging length is illustrated in Fig.7. Internal pressure is only applied to the tube specimen with this setup and it is bulged freely. In the experiment, the initial length of the tube is 200mm, and the bulging length is set at 30mm, 60mm, and 90mm, respectively. Fig.8 shows the experimental results when the tube is bursting with the different bulging length, in which the bursting pressure is 28.7MPa, 24.34MPa, and 22.81MPa, respectively.

FEM simulations based on the Gurson–Tvergaard–Needleman model were carried out in order to examine the experimental results, in which parameters of the Gurson–Tvergaard–Needleman model are selected as Table 3. In the FE model, only half part of the tube is actually analyzed due to symmetry of the problem, as shown in Fig.9. The die and punches are assumed rigid and modelled as discrete rigid surfaces, while the tube is modelled with 18090 S4R shell elements. Contact between the tube and die is modelled using a penalty-based contact algorithm and the coefficient of friction of 0.1 is applied to the contact surface.

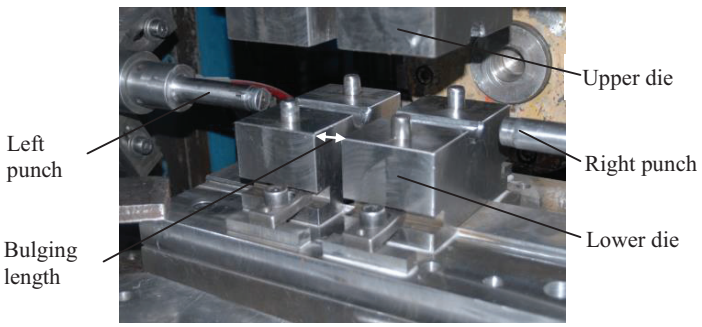

Fig. 7. Experimental set up.

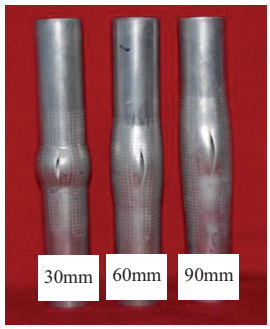

Fig. 8. 5A02 tubes after bursting with different bulging length.

Fig.10 presents the porosity history of the element at the pole of the tube. It can be seen from the figure that the porosities are small before the pressure reaches 20MPa. It can be noticed that under the same internal pressure, a larger porosity at the pole of the tube with a longer bulging length. As demonstrated in the figure, a longer bulging length will accelerate damage development and ductile fracture. When the pressure reaches 22.35MPa, 25.5MPa and 27.9MPa with the bulging length of 90mm, 60mm, and 30mm, the porosity at the pole of the tube reaches the failure porosity f_F =0.0363, which indicates that bursting failure has happened. It can also be seen that the pressure for void coalescence is close to final ductile fracture. Compared with the corresponding experimental results, the errors of predicted bursting pressure based on GTN model are 2.05%, 4.43%, and 2.87%, respectively.

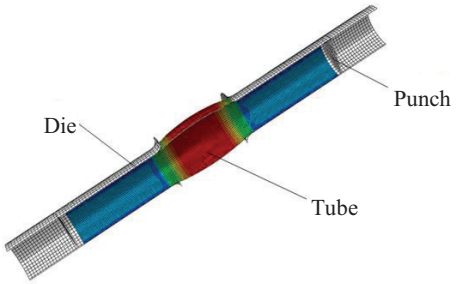

Fig.9. FEM model.

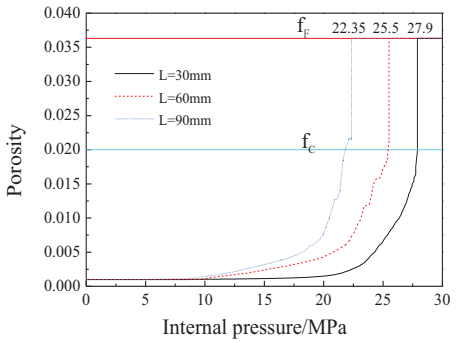

Fig.10. Porosity history versus the internal pressure with different bulging length.

4. Conclusions

1) The parameters in the Gurson–Tvergaard–Needleman model are determined by the tensile tests and the inverse approach. The best-fit parameters for the Gurson–Tvergaard–Needleman model of 5A02 can be assigned as f_0=0.001, f_c=0.02, f_F=0.363, f_N=0.0242, ε_N=0.1, and s_N=0.1.
2) The predicted bursting pressures of free-bulging 5A02 aluminium alloy tubes based on the Gurson–Tvergaard–Needleman model show a good agreement with the experimental results. The maximum error is less than 5%.

Acknowledgement

This work was sponsored by the Scientific Research Foundation for the Returned Overseas Chinese Scholars, State Education Ministry. The authors would like to take this opportunity to express their appreciation.

References

Yuan, S.J., He, Z.B., Liu, G., Wang, X.S., Han, C., 2011. New developments in theory and processes of internal high pressure forming. The Chinese Journal of Nonferrous metals, 10:2523-2533. (in Chinese)

Kim, J., Kang, S.J., Kang B.S., 2003. A prediction of bursting failure in tube hydroforming processes based on ductile fracture criterion. International Journal of Advanced Manufacturing Technology, 22:357–362

Stoughton, B.T., Zhu, X.H., 2004. Review of theoretical models of the strain-based FLD and their relevance to the stress-based FLD. International Journal of Plasticity, 20:1463-1486.

Tvergaard., V., Needleman A., 1984. Analysis of the cup-cone fracture in a round tensile test bar. Acta Metall, 32:157-169

Yan, S.L., Yang,H., Li, H.W., Ren, G.Y., 2014. Experimental study of macro–micro dynamic behaviors of 5A0X aluminum alloys in high velocity deformation. Materials Science&Engineering A. 59:197-206.